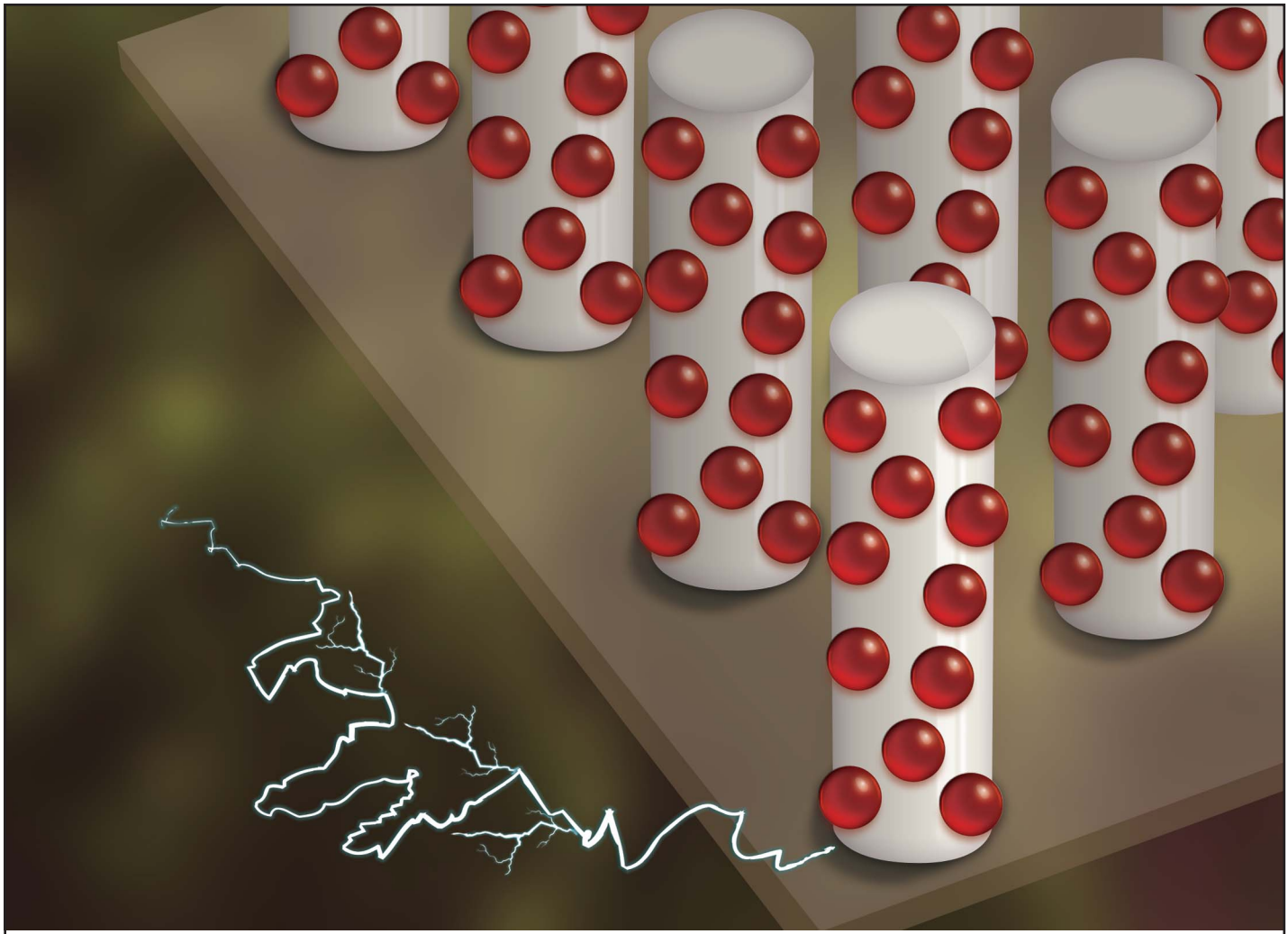

Showcasing the research on quantum dot sensitized solar cells from Prof. J. J. Tian's and Prof. G. Z. Cao's lab, University of Science and Technology Beijing, China, and University of Washington, the United States.

Title: Constructing ZnO nanorod array photoelectrodes for highly efficient quantum dot sensitized solar cells

A ZnO nanorod (NR) array photoelectrode for CdS/CdSe quantum dot cosensitized solar cells (QDSCs) was fabricated by growing on a seeded ITO substrate without using a template or high temperature conditions, which generated a high power conversion efficiency of 3.14%.

As featured in:

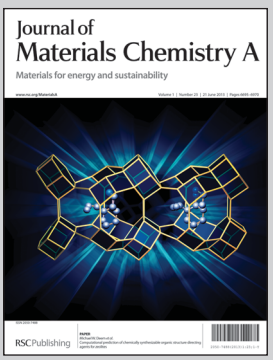

See J. Tian *et al.*,
J. Mater. Chem. A, 2013, **1**, 6770.

RSC Publishing

www.rsc.org/MaterialsA

Registered Charity Number 207890

Journal of Materials Chemistry A

RSC Publishing

PAPER

Constructing ZnO nanorod array photoelectrodes for highly efficient quantum dot sensitized solar cells

Cite this: *J. Mater. Chem. A*, 2013, **1**, 6770

Jianjun Tian,*[ac] Qifeng Zhang,[b] Evan Uchaker,[b] Zhiqiang Liang,[bc] Rui Gao,[b] Xuanhui Qu,[a] Shengen Zhang[a] and Guozhong Cao*[bc]

Received 14th March 2013
Accepted 10th April 2013

DOI: 10.1039/c3ta11056g

www.rsc.org/MaterialsA

This work reports on a ZnO nanorod (NR) array photoelectrode for CdS/CdSe quantum dot cosensitized solar cells (QDSCs), which generated a high power conversion efficiency of 3.14%. ZnO NR arrays were fabricated by growing on a seeded indium-doped tin oxide (ITO) substrate without using a template or high temperature conditions. The ZnO NR served as the backbone for direct electron transport in view of its single crystallinity and high electron mobility. To improve the performance of the QDSC, we introduced a facile chemical surface modification of the ZnO NR array photoelectrodes. The chemical processing not only formed a barrier layer of TiO_2 nanoparticles on the surface of the ZnO NR, which suppresses charge recombination by preventing the electrons in the ZnO conduction band from transferring to the oxidized ions in the electrolyte, but also modified the surface characteristics of the ZnO NR so as to harvest a greater amount of QDs and increase the short current density of the QDSC. As a result, the QDSC assembled with the modified ZnO NR array photoelectrode exhibited a high performance with J_{sc}, V_{oc}, FF and η performance values equal to 9.93 mA cm^{-2}, 0.61 V, 0.52 and 3.14%, respectively.

1 Introduction

Recently, quantum dot-sensitized solar cells (QDSCs) as a cost-effective alternative to silicon-based photovoltaics have attracted considerable attention and shown promise toward the development of next generation solar cells.[1–5] QDSCs can be regarded as derivatives of dye-sensitized solar cells (DSCs); however, they use semiconductor quantum dots (QDs) instead of organic dyes as photosensitizers.[6–8] Compared to organic dyes, narrow-band-gap semiconductor QDs, such as CdS,[9,10] CdSe,[11,12] PbS[13] and InAs,[14] as next-generation sensitizers are considered more promising because of their extraordinary optical and electrical properties in terms of (1) tunable band-gap dependent on QD size, (2) large extinction coefficient, (3) high stability toward water and oxygen and (4) generation of multiple excitons with single-photon absorption.[15–17] The theoretical photovoltaic conversion efficiency of QD-sensitized solar cells can extend up to 44% in view of the multiple exciton generation (MEG) effect as a result of the quantum confinement effect of QDs.[17,18]

As a wide band-gap semiconductor for the sensitizer scaffold, conventional TiO_2 and ZnO porous nanocrystalline films had been used in both DSCs and QDSCs. Our previous research reported[17] that QDs experienced difficulty penetrating into the inner pores of the films, leading to several issues: (1) the direct exposure of the TiO_2 film to the electrolyte resulting in a serious degree of recombination between the electrons in the TiO_2 and the holes in the electrolyte; (2) less QD loading in the films. Open structures, such as nanorods (NRs), nanowires (NWs) and nanotubes, can facilitate the distribution of QDs from the surface to the interior of the films and enhance the QD loading. ZnO is considered an excellent candidate material for photoelectrodes due to its high electron mobility.[19–21] In addition, ZnO can easily form the anisotropic structures used for NR and NW arrays. For the structure of ZnO arrays, ZnO serves as the backbone for direct electron transport by providing short transport distances. Some studies have already demonstrated the use of ZnO nanowire arrays for application in QDSCs.[22–25] However, the efficiency of ZnO based QDSCs is lower than that of TiO_2 based counterparts, likely due to high surface charge recombination in the case of ZnO. In DSCs, it has been proven that the charge recombination can be effectively reduced by introducing a barrier layer on the ZnO surface.[26–30] The barrier layer usually has a more negative conduction band edge than that of ZnO, or creates a dipole at the interface to shift the band edge so as to suppress surface charge recombination.[28] Although the charge recombination process in QDSCs was thought to be somewhat different from that in DSCs,[31] the

[a]*Institute of Advanced Material and Technology, University of Science and Technology Beijing, 100083, P.R. China. E-mail: tianjianjun@mater.ustb.edu.cn; Fax: +86-10-62333375; Tel: +86-10-82376835*

[b]*Department of Materials and Engineering, University of Washington, Seattle, WA 98195-2120, USA. E-mail: gzcao@u.washington.edu; Fax: +1-206-543-3100; Tel: +1-206-616-9084*

[c]*Beijing Institute of Nanoenergy and Nanosystems, Chinese Academy of Sciences, 100085, P.R. China. E-mail: gzcao@binn.cas.cn*

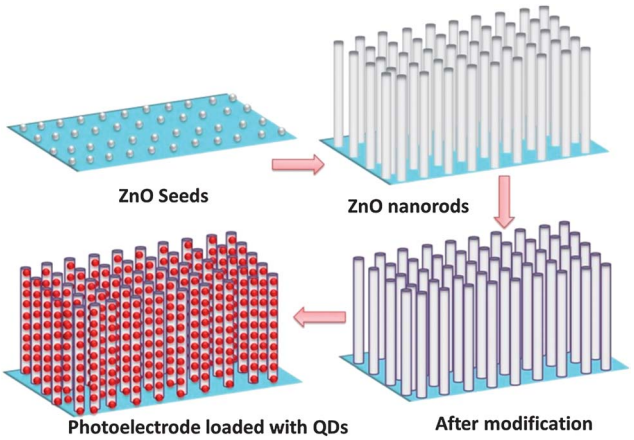

Fig. 1 Schematic illustration of the fabrication process of ZnO NR array photoelectrodes for QDSCs.

method of introducing a shell layer as well as an energy barrier to prevent the electrons from transferring from the oxide to the electrolyte is believed to be effective in improving the performance of QDSCs. In addition to forming an energy barrier, the barrier layer may also alter the surface energy of ZnO, thus enhancing the QD loading of ZnO-based QDSCs which suffer from relatively low QD loading leading to low J_{sc} and efficiency.[32]

In this work, we report a chemical processing method for the surface modification of ZnO NR array photoelectrodes to suppress the charge recombination and increase the QD loading. Fig. 1 illustrates the formation steps of the ZnO NR array and the resulting novel photoelectrodes for QDSCs. Firstly, ZnO NR arrays can be fabricated by growing on seeded indium-doped tin oxide (ITO) without the use of a template or high temperature conditions. ZnO NRs grown along the (0001) direction[33] were well aligned perpendicularly to the ITO substrate. Following this initial step, the ZnO NR arrays were modified using a solution of H_3BO_3 and $(NH_4)_2TiF_6$. ZnO reacted with H_3O^+ and the surface ions were dissolved. At the same time, TiO_2 was deposited on the surface of ZnO by the hydrolysis of TiF_6^{2-}. Finally, CdS and CdSe were directly grown on the ZnO NR array surface by successive ionic layer adsorption and reaction (SILAR) and chemical bath deposition (CBD) processes, respectively. As a result of this fabrication process, the power conversion efficiency of the QDSCs increases from 1.54% for ZnO NR arrays without modification to 3.14% for ZnO NR arrays after modification.

2 Experimental

2.1 Preparation of ZnO NR array films

The ITO substrates were spin coated with 0.60 M zinc acetate in a solution of 2-methoxyethanol and monoethanolamine to form a seed layer of ZnO, followed by heat treatment at 300 °C for 10 min. The seeded ITO substrates were placed in an aqueous solution containing 0.02 M $Zn(NO_3)_2$ and hexamethylenetetramine aqueous solution at 95 °C for 40 h, resulting in ZnO NRs with a length of ~8 μm and a diameter of ~150 nm. Subsequently, ZnO NR arrays grown on the ITO were thoroughly rinsed with deionized water (DI) to remove any residual chemicals and were calcined at 300 °C for 30 min.

2.2 Modification process of ZnO NR arrays

The ZnO NR arrays were immersed in an aqueous solution of 0.04 M H_3BO_3 and 0.1 M $(NH_4)_2TiF_6$ at room temperature for 30 min. The substrate was drained from the reaction solution and washed several times with deionized water. The modified ZnO NR arrays were then calcined at 350 °C for 30 min.

2.3 Fabrication of CdS/CdSe sensitized solar cells

For the growth of CdS quantum dots, the substrates were first immersed into a 0.1 M cadmium nitrate ($Cd(NO_3)_2$) methanol solution for 1 min. Successively, the substrates were dipped into a 0.1 M sodium sulfide (Na_2S) methanol solution for another 1 min to allow S^{2-} to react with the pre-adsorbed Cd^{2+}, leading to the formation of CdS. This procedure was denoted as one SILAR cycle. In total, 5 SILAR cycles were employed to obtain a suitable amount of CdS on the TiO_2 film. In a subsequent step, CdSe was deposited on the CdS coated substrates through a CBD method. In brief, 0.1 M sodium selenosulphate (Na_2SeSO_3), 0.1 M cadmium acetate ($Cd(CH_2COO)_2$) and 0.2 M trisodium salt of nitrilotriacetic acid ($N(CH_2COONa)_3$) were mixed together at a volume ratio of 1 : 1 : 1. The CdS coated substrates were then vertically immersed into the solution for the deposition of the CdSe layer under dark conditions at 24 °C for 3 h. After CdSe deposition, a ZnS passivation layer was deposited by two SILAR cycles by soaking in an aqueous solution containing 0.1 M zinc nitrate and 0.1 M sodium sulfide, which act as Zn^{2+} and S^{2-} sources, respectively. The electrolyte employed in this study was composed of 1 M S and 1 M Na_2S in deionized water. The counter electrode was a Cu_2S film fabricated on brass foil. The preparation of the Cu_2S electrode can be described as follows: brass foil was immersed in 37% HCl at 70 °C for 5 min, then rinsed with water and dried in air. Following this step, the etched brass foil was dipped into 1 M S and 1 M Na_2S aqueous solution, resulting in a black Cu_2S layer forming on the foil.

2.4 Characterization

The morphology of the ZnO arrays was characterized by scanning electron (SEM, JSM-7000) and transmission electron (TEM, Tecnai G2 F20) microscopy. The photovoltaic properties were measured using an HP 4155A programmable semiconductor parameter analyzer under AM 1.5 simulated sunlight with a power density of 100 mW cm^{-2}. Optical absorption (Perkin Elmer Lambda 900 UV/VIS/IR Spectrometer) was used to study the light absorption properties of the samples. Electrochemical impedance spectroscopy (EIS) was carried out using a Solartron 1287A coupled with a Solartron 1260 FRA/impedance analyzer to investigate the electronic and ionic processes in the QDSCs.

3 Results and discussion

The morphology of the nanowire arrays was examined with a SEM. As displayed in Fig. 2a and b, the ZnO NR arrays have a highly oriented 1D structure (preferential growth along the

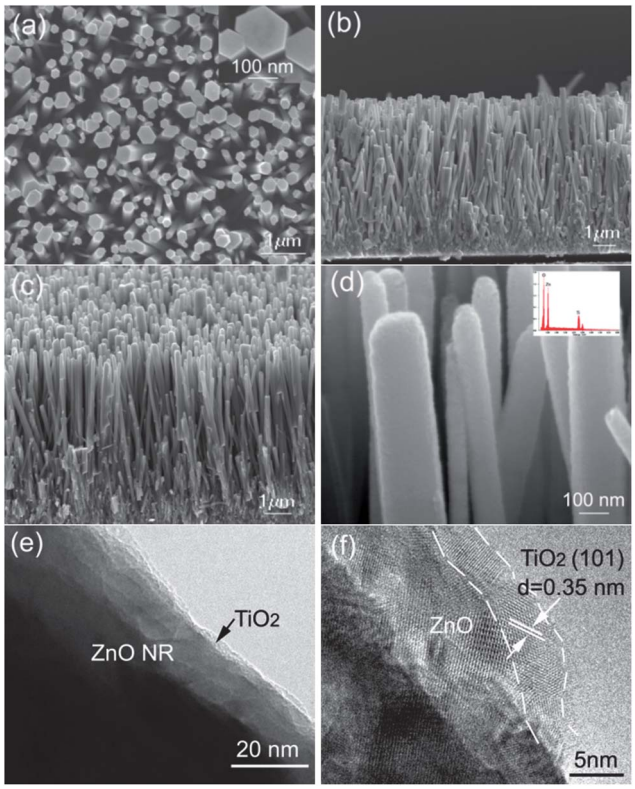

Fig. 2 (a) and (b) SEM images of ZnO NR arrays, showing the ZnO NRs with an average diameter and length of 100 nm and 8 μm, respectively; (c) low and (d) high magnification SEM images of the modified ZnO NR arrays; the inset shows EDS spectra of modified ZnO NR arrays; (e) TEM and (f) HRTEM images of the modified ZnO NR, showing the ZnO NR coated with TiO_2 nanoparticles with a size of 4–5 nm.

(0001) *c*-axis) with a typical diameter in the range of 50–150 nm and a length of approximately 8 μm. Fig. 2c and d show the low and high magnification SEM images of the ZnO NR arrays after modification, respectively. It can be seen that the edges and corners of the ZnO NRs disappear due to the dissolution of the ZnO NR surfaces according to the following equation:[34]

$$ZnO + 2H_3O^+ \rightarrow Zn^{2+} + 3H_2O \quad (1)$$

where H_3O^+ ions derive from the reaction of TiF_6^{2-} and H_3BO_3 *via* the following equations:

$$TiF_6^{2-} + 2H_2O \leftrightarrow TiO_2 + 6F^- + 4H^+ \quad (2)$$

$$H_3BO_3 + 4H^+ + 4F^- \leftrightarrow BF_4^- + H_3O^+ + 2H_2O \quad (3)$$

The ZnO NRs dissolve into the solution by reacting with H_3O^+ which boosts the hydrolysis of TiF_6^{2-} and results in the deposition of TiO_2 onto the surface of the ZnO NRs. With the dissolving of ZnO, TiO_2 deposits gradually onto the fresh ZnO surface, forming a thin layer on the ZnO surface. Energy-dispersive X-ray spectroscopy (EDS) (Fig. 2d inset) shows the presence of O, Zn and Ti elements, verifying the formation of the TiO_2 layer on the surface of the ZnO NRs. Compared to the ZnO NRs without modifying treatment, the edges of the modified ZnO NRs become "rough", indicating that the ZnO surface characteristics have been altered by the dissolution of ZnO and deposition of TiO_2. The "rough" surface would be helpful for harvesting QDs. Fig. 2e and f displays TEM and HRTEM images of the modified ZnO NR, showing the NR coated with TiO_2 nanoparticles that are 4–5 nm in diameter. The figure indicates that the thickness of the TiO_2 layer is around 5 nm.

Fig. 3a is the TEM image of a ZnO NR loaded with QDs, clearly revealing that the ZnO NR is surrounded by small particles 4–6 nm in size. The small particles can be confirmed as CdS/CdSe/TiO_2 structures by HRTEM imaging (Fig. 3b), indicating that the "rough" edge resulted from CdSe and CdS QDs adsorbing on the TiO_2-coated ZnO NRs. EDS analyses were performed to study the distribution of QDs and TiO_2 on the surface of the ZnO NRs. As Fig. 3c–e show, the distribution of Ti and Se elements is consistent with that of elemental Zn. Fig. 3f shows the overlapped elemental image mapping distribution of Zn, Ti and Se, indicating that the Zn NR is conformally coated by Ti and Se elements.

The optical absorption spectra of two ZnO NR arrays loaded with QDs are shown in Fig. 4. The results reveal that the absorbance of the ZnO NR arrays after modification is higher than that of ZnO NR arrays without modifying treatment. The high absorbance of the photoelectrode indicates that a greater amount of QDs can be acquired. The previous results might be attributed to (1) changing the surface energy and surface profile

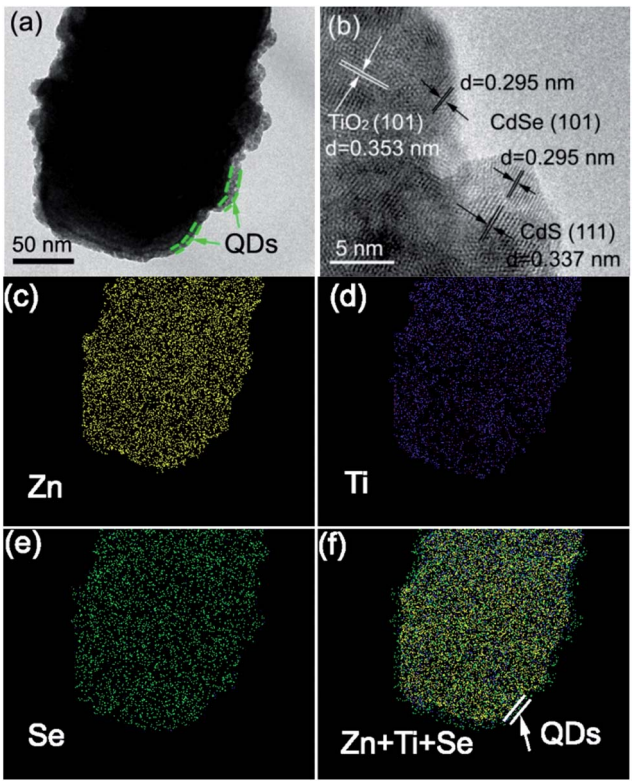

Fig. 3 TEM (a) and HRTEM (b) images of ZnO NR arrays loaded with QDs; (c), (d), (e) and (f) are the elemental maps of the modified ZnO NRs, displaying the Zn, Ti, Se and Zn + Ti + Se spatial elemental distribution, respectively.

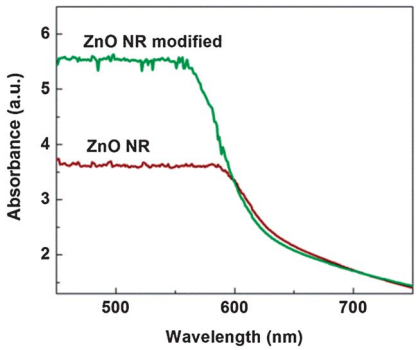

Fig. 4 Diffuse reflectance spectra (DRS) of ZnO NR array photoelectrodes loaded with QDs.

of the photoelectrode by modifying treatment for harvesting a greater amount of QDs; and (2) increasing the surface area of the photoelectrode by deposition of TiO_2 nanoparticles to favor high QD loadings.

Fig. 5 depicts the structure of the QDSC and charge recombination pathways in the solar cell. The cell structure of the quantum dot sensitized solar cell (Fig. 5a) consists of the ZnO NR film array, QD sensitizer, polysulfide electrolyte and counter electrode; the ZnO NR arrays served as the backbone for direct electron transport providing short transport distances in the QDSC. Under operating conditions, photons are captured by the QDs yielding electron–hole pairs that are rapidly separated to electrons and holes at the interface between the nanocrystalline oxide and QDs. The electrons are injected into the oxide and holes are released by redox couples (S^{2-}/S_n^{2-}) in the electrolyte. Compared to the case of dye sensitized solar cells, the recombination in QDSCs is more complicated in view of there being more pathways for the occurrence of charge recombination:[8,32] (A) recombination of electrons in the QD conduction band with holes in the QD valence band; (B) recombination of electrons with the electron acceptors in the electrolyte; (C) back electron injection from ZnO to the electrolyte; and (D) back electron injection from ZnO to QDs. Among these pathways, processes (A) and (B) can be ignored due to the highly efficient charge separation.[32] Thus, recombination pathways (C) and (D) can be considered as the main factors that affect the performance of a QDSC, depending on the interface resistance of the oxide with the electrolyte and QDs. The thin layer of TiO_2 can increase the interface resistance and lead to a reduction in the recombination through mechanisms (C) and (D). The charge transport properties and recombination of QDSCs can be explained using electrochemical impedance spectroscopy (EIS).

Fig. 6 shows the impedance spectra of the QDSCs measured under forward bias (−0.6 V) and dark conditions. In Fig. 6a, the large semicircle corresponds to the electron transfer at the photoelectrode–QDs–electrolyte interface and transport in the photoelectrode (R_{ct}).[35] A fitting result of the impedance spectra is listed in Table 1. The R_{ct} reflects electron recombination corresponding to processes (C) and (D) in Fig. 5b. Compared to the ZnO NR array based QDSC, the R_{ct} of the ZnO NR arrays after modification increases from 80.1 Ω to 129.2 Ω. As the charge transfer resistance at the photoelectrode–electrolyte interface (R_{ct}) includes the resistances of both the ZnO and shell layer, the total charge transfer resistance can be expressed by eqn (4):[32]

$$R_{total} = R_{ZnO} + R_{shell} \quad (4)$$

where R_{ZnO} and R_{shell} are the electron transfer resistances induced by the ZnO and TiO_2 shell, respectively. These results indicate that electrons in the photoelectrode after modification are more difficult to recombine in view of the high R_{ct}. Fig. 6b shows the Bode plots of the QDSCs with different photoelectrodes. The curved peak of the spectrum can be used to

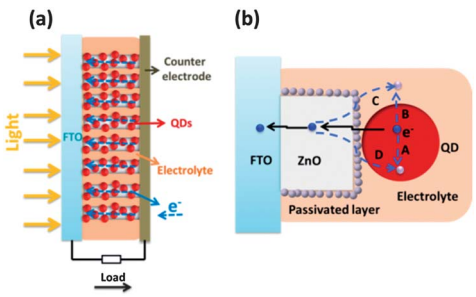

Fig. 5 Schemes of the (a) QDSC structure (b) and charge recombination pathways.

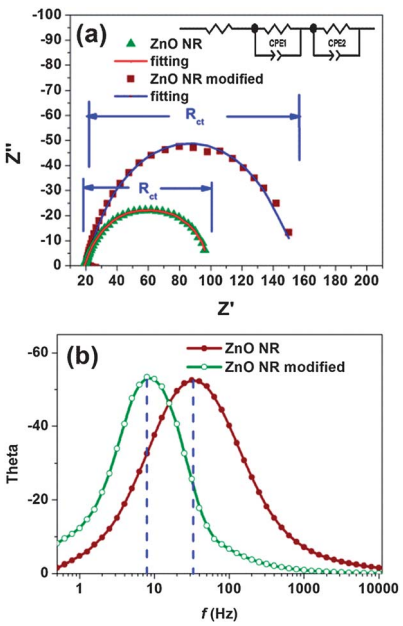

Fig. 6 (a) Nyquist plot curves and (b) Bode plot curves of QDSCs under forward bias (−0.6 V) and dark conditions.

Table 1 Electrochemical impedance results of QDSCs

Samples	R_1 (Ω)	R_{ct} (Ω)	τ_n (mS)
ZnO NR	19.1	80.1	5.0
ZnO NR modified	22.3	129.2	20.1

determine the electron lifetime in the ZnO according to eqn (5):[36]

$$\tau_n = \frac{1}{2\pi f_{\min}} \quad (5)$$

The corresponding results are listed in Table 1, revealing that the electron lifetime of the device with the ZnO photoelectrode after modification is up to 20.1 ms, which is much longer than that of the photoelectrode without modifying treatment (5.0 ms). In other words, the lifetime of electrons in the conduction band is prolonged due to the modification.

It is known that the charge recombination and electron lifetime have an obvious impact on V_{oc}, FF and η for DSCs, and this is the case for QDSCs. The V_{oc} can be expressed by eqn (6):[37,38]

$$V_{oc} = \frac{RT}{\beta F}\ln\left(\frac{AI}{n_0 k_b [S_n^-] + n_0 k_r [D^+]}\right) \quad (6)$$

where R is the molar gas constant, T is the temperature, F is the Faraday constant, β is the reaction order for S_n^- and electrons, A is the electrode area, I is the incident photon flux, n_0 is the concentration of accessible electronic states in the conduction band and k_b and k_r are the kinetic constants of the back-reaction of the injected electrons with the polysulfide electrolyte and the recombination of these electrons with oxidized QDs (D^+), respectively. Considering that ω_{max} ($1/f_{min}$) is the same as the back-reaction constant (k_b), and that the V_{oc} is dependent logarithmically on f_{min}, it is clear that the V_{oc} value increases with the decrease of the back-reaction constant (same as f_{min}). From Fig. 6b, the device with the ZnO photoelectrode after modification has much lower f_{min} than that using the photoelectrode that did not undergo the modification process. Subsequently, according to eqn (6), the device with the photoelectrode after modification should have higher V_{oc}. The charge transfer resistance at the photoelectrode–electrolyte interface, denoted as R_{ct} in Fig. 6a, can be considered as part of a shunt resistance (R_{sh}) because it behaves like a diode with the applied bias voltage.[26] The R_{sh} relates to the FF according to eqn (7):[26]

$$FF = FF_0(1 - 1/R_{sh}) \quad (7)$$

where FF_0 is the theoretical maximum FF. From the EIS results, it can be inferred that the FF increase for the QDSC is a result of an increase in R_{sh}. Following previous discussions, it is evident that this modification contributes towards improving the J_{sc}, FF and V_{oc} of the QDSCs.

Fig. 7 shows the J–V curves for the solar cells measured under the illumination of one sun (AM 1.5, 100 mW cm^{-2}). The performance parameters of the solar cells are listed in Table 2. The QDSC assembled with modified ZnO NR arrays exhibits high performance: J_{sc} = 9.93 mA cm^{-2}, V_{oc} = 0.61 V, FF = 0.52 and η = 3.14%. Compared with the photoelectrode without modifying treatment, the modified ZnO NR array photoelectrode displays increases in V_{oc}, J_{sc}, FF and η by 5%, 35%, 44% and 104%, respectively. Therefore, the performance of the QDSC assembled with ZnO NR arrays can be enhanced *via* a chemical modification process by introducing a barrier layer for suppressing surface charge recombination back to the electrolyte and changing the surface characteristics of the ZnO NR for harvesting a greater amount of QDs.

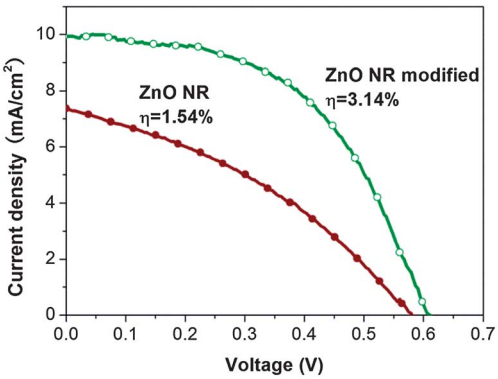

Fig. 7 *J–V* curves of the modified and unmodified ZnO NR array photoelectrode based QDSCs under simulated AM 1.5, 100 mW cm^{-2} sunlight.

Table 2 Properties of ZnO NR array photoelectrode based QDSCs

Samples	V_{oc} (V)	J_{sc} (mA cm^{-2})	FF	η (%)
ZnO NR	0.58	7.36	0.36	1.54
ZnO NR modified	0.61	9.93	0.52	3.14

4 Conclusion

A ZnO nanorod array photoelectrode for CdS/CdSe quantum dot cosensitized solar cells was examined in this investigation. The ZnO NR arrays were fabricated by growth on seeded ITO without using a template or high temperature conditions. The ZnO NR served as the backbone for direct electron transport in view of its single crystallinity and high electron mobility. To improve the performance of the QDSC, we introduced a facile chemical surface modification of the ZnO NR array photoelectrode. The chemical process not only formed a barrier layer of TiO_2 nanoparticles on the surface of the ZnO NR to suppress the charge recombination by preventing the electrons in the conduction band of ZnO from transferring to the oxidized ions in the electrolyte, but also changed the surface characteristics of the ZnO NR so as to harvest a greater amount of QDs and increase the short current density of the QDSC. As a result, the QDSC assembled with the modified ZnO NR array photoelectrode exhibited a high performance as exemplified by the device parameters of merit: J_{sc} = 9.93 mA cm^{-2}, V_{oc} = 0.61 V, FF = 0.52 and η = 3.14%. In addition, the efficiency of QDSCs is kept at a high value (≥3%) and decreases slightly (<5%) after several days in ambient conditions, indicating their good stability. It should also be noted that the decrease may most likely be due to the evaporation of electrolyte solvent, not the degradation of QDs.

Acknowledgements

This work was supported by the National Science Foundation of China (51004011 and 51174247) and the Fundamental Research

Funds for the Central Universities (FRF-TP-12-153A). This work is also supported in part by the National Science Foundation (DMR 1035196), the University of Washington TGIF grant and the Royalty Research Fund (RRF) from the Office of Research at University of Washington.

Notes and references

1 H. Tada, M. Fujishima and H. Kobayashi, *Chem. Soc. Rev.*, 2011, **40**, 4232–4243.
2 P. K. Santra and P. V. Kamat, *J. Am. Chem. Soc.*, 2012, **134**, 2508–2511.
3 M. A. Hossain, J. R. Jennings, Z. Y. Koh and Q. Wang, *ACS Nano*, 2011, **5**, 3172–3181.
4 J. Ryu, S. H. Lee, D. H. Nam and C. B. Park, *Adv. Mater.*, 2011, **23**, 1883–1888.
5 T. Sugaya, O. Numakami, R. Oshima, S. Furue, H. Komaki, T. Amano, K. Matsubara, Y. Okano and S. Niki, *Energy Environ. Sci.*, 2012, **5**, 6233–6237.
6 J. H. Bang and P. V. Kamat, *Adv. Funct. Mater.*, 2010, **20**, 1970–1976.
7 V. Gonzalez-Pedro, X. Xu, I. Mora-Sero and J. Bisquert, *ACS Nano*, 2010, **4**, 5783–5790.
8 X.-Y. Yu, J.-Y. Liao, K.-Q. Qiu, D.-B. Kuang and C.-Y. Su, *ACS Nano*, 2011, **5**, 9494–9500.
9 J. Kim, H. Choi, C. Nahm, J. Moon, C. Kim, S. Nam, D.-R. Jung and B. Park, *J. Power Sources*, 2011, **196**, 10526–10531.
10 S. Panigrahi and D. Basak, *J. Colloid Interface Sci.*, 2011, **364**, 10–17.
11 I. Robel, V. Subramanian, M. Kuno and P. V. Kamat, *J. Am. Chem. Soc.*, 2006, **128**, 2385–2393.
12 Q. Shen, J. Kobayashi, L. J. Diguna and T. Toyoda, *J. Appl. Phys.*, 2008, **103**, 084304.
13 R. Plass, S. Pelet, J. Krueger, M. Gratzel and U. Bach, *J. Phys. Chem. B*, 2002, **106**, 7578–7580.
14 P. Yu, K. Zhu, A. G. Norman, S. Ferrere, A. J. Frank and A. J. Nozik, *J. Phys. Chem. B*, 2006, **110**, 25451–25454.
15 G. Zhu, L. Pan, T. Xu and Z. Sun, *ACS Appl. Mater. Interfaces*, 2011, **3**, 3146–3151.
16 Y. L. Lee and Y. S. Lo, *Adv. Funct. Mater.*, 2009, **19**, 604–609.
17 J. J. Tian, R. Gao, Q. F. Zhang, S. G. Zhang, Y. W. Li, J. L. Lan, X. H. Qu and G. Z. Cao, *J. Phys. Chem. C*, 2012, **116**, 18655–18662.
18 T. L. Li, Y. L. Lee and H. Teng, *Energy Environ. Sci.*, 2012, **5**, 5315–5324.
19 T. P. Chou, Q. F. Zhang, G. E. Fryxell and G. Z. Cao, *Adv. Mater.*, 2007, **19**, 2588–2592.
20 Q. F. Zhang and G. Z. Cao, *J. Mater. Chem.*, 2011, **21**, 6769–6774.
21 Q. F. Zhang, T. R. Chou, B. Russo, S. A. Jenekhe and G. Z. Cao, *Angew. Chem., Int. Ed.*, 2008, **47**, 2402–2406.
22 M. Seol, H. Kim, Y. Tak and K. Yong, *Chem. Commun.*, 2010, **46**, 5521–5523.
23 M. Seol, E. Ramasamy, J. Lee and K. Yong, *J. Phys. Chem. C*, 2011, **115**, 22018–22024.
24 C.-Z. Yao, B.-H. Wei, L.-X. Meng, H. Li, Q.-J. Gong, H. Sun, H.-X. Ma and X.-H. Hu, *J. Power Sources*, 2012, **207**, 222–228.
25 T. Bora, H. H. Kyaw and J. Dutta, *Electrochim. Acta*, 2012, **68**, 141–145.
26 K. Park, Q. F. Zhang, B. B. Garcia and G. Z. Cao, *J. Phys. Chem. C*, 2011, **115**, 4927–4934.
27 K. Park, Q. F. Zhang, B. B. Garcia, X. Y. Zhou, Y. H. Jeong and G. Z. Cao, *Adv. Mater.*, 2010, **22**, 2329–2332.
28 M. Law, L. E. Greene, A. Radenovic, T. Kuykendall, J. Liphardt and P. D. Yang, *J. Phys. Chem. B*, 2006, **110**, 22652–22663.
29 M. L. Wang, C. G. Huang, Y. G. Cao, Q. J. Yu, Z. H. Deng, Y. Liu, Z. Huang, J. Q. Huang, Q. F. Huang, W. Guo and J. K. Liang, *J. Phys. D: Appl. Phys.*, 2009, **42**, 155104.
30 N. O. V. Plank, I. Howard, A. Rao, M. W. B. Wilson, C. Ducati, R. S. Mane, J. S. Bendall, R. R. M. Louca, N. C. Greenham, H. Miura, R. H. Friend, H. J. Snaith and M. E. Welland, *J. Phys. Chem. C*, 2009, **113**, 18515–18522.
31 I. Mora-Sero, S. Gimenez, F. Fabregat-Santiago, R. Gomez, Q. Shen, T. Toyoda and J. Bisquert, *Acc. Chem. Res.*, 2009, **42**, 1848–1857.
32 J. J. Tian, Q. F. Zhang, L. L. Zhang, R. Gao, L. F. Shen, S. G. Zhang, X. H. Qu and G. Z. Cao, *Nanoscale*, 2013, **5**, 936–943.
33 Z. L. Wang, *Mater. Sci. Eng., R*, 2009, **64**, 33–71.
34 S. Yodyingyong, X. Y. Zhou, Q. F. Zhang, D. Triampo, J. T. Xi, K. Park, B. Limketkai and G. Z. Cao, *J. Phys. Chem. C*, 2010, **114**, 21851–21855.
35 N. Koide, A. Islam, Y. Chiba and L. Y. Han, *J. Photochem. Photobiol., A*, 2006, **182**, 296–305.
36 R. Kern, R. Sastrawan, J. Ferber, R. Stangl and J. Luther, *Electrochim. Acta*, 2002, **47**, 4213–4225.
37 Q. Wang, S. Ito, M. Gratzel, F. Fabregat-Santiago, I. Mora-Sero, J. Bisquert, T. Bessho and H. Imai, *J. Phys. Chem. B*, 2006, **110**, 25210–25221.
38 K. Lee, S. W. Park, M. J. Ko, K. Kim and N. G. Park, *Nat. Mater.*, 2009, **8**, 665–671.